Beyond phase error compensation: pixel mapping-based error correction for high-accuracy 3D surface measurement

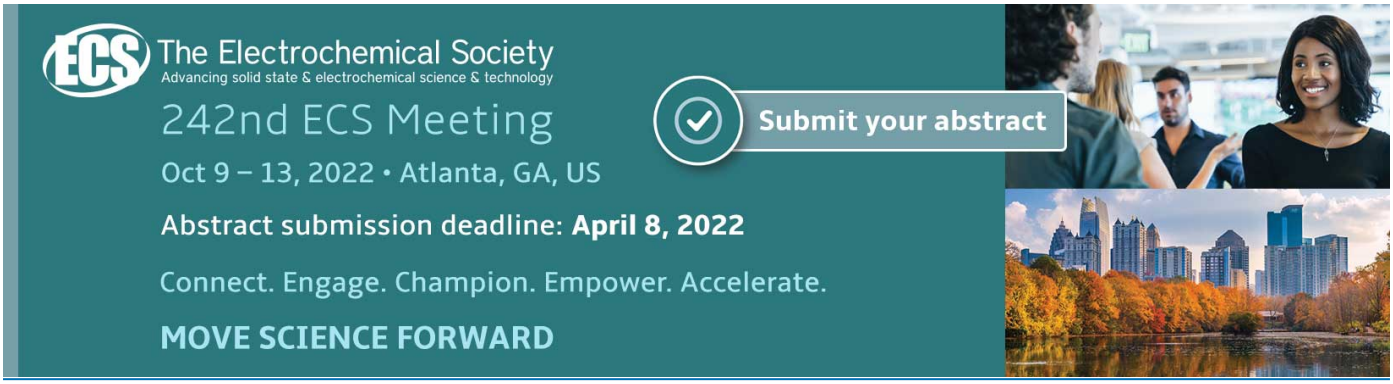

IOP Publishing Measurement Science and Technology
Meas. Sci. Technol. 31 (2020) 065007 (10pp) https://doi.org/10.1088/1361-6501/ab6675

Beyond phase error compensation: pixel mapping-based error correction for high-accuracy 3D surface measurement

Zaixing He[1], Peilong Li[1], Xinyue Zhao[1], Shuyou Zhang and Jianrong Tan

School of Mechanical Engineering, the State Key Lab of Fluid Power & Mechatronic Systems, Zhejiang University, Hangzhou, Zhejiang 310027, People's Republic of China

E-mail: zhaoxinyue@zju.edu.cn

Received 12 November 2019, revised 16 December 2019
Accepted for publication 31 December 2019
Published 13 March 2020

Abstract

In optical-based phase-shifting 3D surface profilometry, phase errors are inevitable and lead to final measurement errors. Error compensation, based on pre-estimated phase errors, is an effective technique to alleviate the phase errors. However, the static and inaccurate nature of the pre-estimated errors lead to an implicit limit to the compensation accuracy. Furthermore, the procedures for error pre-estimation require additional projections, which reduces convenience in practice. In this paper, a novel pixel mapping-based error correction method is proposed. Different from compensation, with the proposed pixel-mapping errors inside each camera pixel can be directly corrected by online replacing with its corresponding ground-truth values input in the projector. This replacement technique is the key idea of our method, which establishes a shortcut to error-free ground-truth values, skipping the traditional laborious and imprecise compensation procedures. To achieve pixel-mapping, an optimization method is proposed and no additional projections are required. A phase error formulation is also introduced in the optimization method to eliminate the phase error distrubance when computing the pixel mapping. Extensive experimental results are shown to demonstrate that the phase accuracy can be obviously improved after utilizing the proposed method.

Keywords: phase-shifting profilometry (PSP), phase measurement, phase error, fringe analysis

(Some figures may appear in colour only in the online journal)

1. Introduction

Phase-shifting profilometry (PSP) has been widely employed in industry, such as reverse engineering, defect detection, object recognition, 3D printing, etc, as one of the most effective and convenient non-contact methods for 3D shape measurement [1–4]. Typically, a PSP system consists of a projector and a camera. The projected fringe patterns captured by a camera are utilized for coding the phase information [5]. The phase information can be mapped to the depth information through triangulation [12]. To extract the phase information, a 4-step phase-shifting (PS) algorithm is commonly used, which can provide relatively high measurement accuracy [12]. However, as many projectors and cameras are fabricated to be nonlinear for better vision effect [7, 25, 26], and with sensor noise and defects [6], the captured images inevitably deviate from the ideal fringe patterns, which may result in considerable phase coding errors.

To alleviate these errors, many methods have been proposed by way of compensation. These methods can be classified into three categories: the passive methods, the active methods and the inverse-cancellation methods.

The passive methods compensate the captured patterns using *a priori* information pre-calibrated. In a passive method, the captured images are modified. Typically, look-up table (LUT) methods pertain to passive methods [8, 10, 11].

[1] Authors contributed equally to this work.

The LUT method was firstly put forward by Zhang and Huang [8]. By comparing the input truth grey and output distorted grey, the nonlinear gamma (γ) errors were pre-calibrated and stored in a table, which can be further used for reducing phase errors for the three-step PS algorithm. Zhang and Yau [10] proved that this method is also generic for any PS algorithm. Moreover, they simply modified the previous LUT method by improving the previous calibration of the γ, and freed the restriction that γ should be monotonic. To further promote the usability of the LUT method, a phase-shifting uniform-phase algorithm (PSUPA) was proposed in [11].

The active methods compensate the projected patterns to finally capture a nearly error-free pattern [13–17]. To determine what should be superimposed on the projected patterns, these methods utilize a certain error-distribution model as a reference. In [7, 14], the phase errors was approximated as a sum of sinusoidal terms with frequencies orderly from low to high. According to this model, a black-box method [17], and an inverse function analysis (IFA) method to compensate phase errors [15] were proposed. In [16], a more thorough theoretical error-distribution model was proposed, taking into account both the projector defocus and the nonlinear gamma effect. A model that further extended the application of the active methods to be used for arbitrary-step PS algorithm was put forward in [13].

The inverse-cancellation methods have been proposed recently, and were reported to be more convenient than the former two methods. It constructs another error-distortion image with negative signs for compensation. The inverse-phase (IP) method utilized a proper phase-offset to construct another set of projected patterns that produce reverse-sign errors in the two captured images [18, 27]. Therefore, the errors can be compensated by averaging values in the two phase-offset images.

The error compensation methods have effectively improved the 3D measurement accuracy, and extended the industrial application of 3D PSP technology. However, nowadays' industry is demanding higher precision and convenience. Error compensation becomes difficult to meet these demands. Two important reasons are as follows.

(1) The accuracy of error compensation is limited.

Regardless of the type of compensation method, the essence is to pre-estimate phase errors and then use it to compensate the subsequent phase errors [9, 17]. Theoretically speaking, it cannot completely eliminate the error since the pre-estimated phase errors are always different from the actual situation. In short, there is an implicit accuracy limit for compensation due to the static and inaccurate nature of the pre-estimated phase errors. It is difficult to further significantly improve the accuracy by proposing new compensation methods.

(2) The convenience of compensation is relatively low.

The convenience metioned in this pater is maily about the number of additional projections. For currently available phase error compensation methods, numbers of specially designed additional projections are required. These specially designed additional projections are important for error-estimation. For the active and passive methods, the calibration procedures significantly increase the projection numbers. For the IP method, the number of additional projections can be decreased but are still needed.

Therefore, correcting errors in an effective yet more convenient way is still a challenging issue. In this paper, a pixel mapping-based approach is proposed. Different from error compensation, the proposed method attempts to use the ground-truth values that input into the projector to directly correct the phase errors, instead of using the pre-estimated phase errors. To achieve this goal, the key idea is to construct a corresponding relationship (the pixel-mapping), between the projector pixel and its related camera pixel associated with the same object point. As the ground-truth phase value inside each projector pixel is known, if the pixel-mapping could be established, the error-distorted phases inside each camera pixel could be directly corrected in an online replacement way. This replacement way is the key idea of our method, which establishes a shortcut to error-free values, skipping the traditional laborious and imprecise compensation procedures.

The challenge of the proposed method mainly lies in how to simply establish the pixel mapping. Generally, binary Gray code patterns and the line-shifting patterns can be used for establishing a pixel mapping [19–22]. However, for PSP, these methods mean that additional projections are required, which are not suitable for a convenient measurement task. In this paper, a novel optimization method is proposed to establish the pixel mapping. We introduce a phase error formulation in this optimization aiming to eliminate the disturbance of phase error to obtain an accurate pixel mapping. In addition, only the sinusoidal PS patterns required for the PSP method are required for retrieving the pixel-mapping. In other words, no additional projections are required for the proposed method. Based on this, the total required projections of our method are shrunk to a minimum, which provides further improvement in practicality and convenience.

This paper is organized as follows. Section 2 presents the principle of the proposed pixel-mapping-based error correction method. Experiments that verify the proposed method are presented in section 3. A conclusion and possible future works are offered in section 4.

2. Pixel mapping-based error correction approach based on PS patterns

As mentioned above, the pixel mapping is crucial for improving PSP measurement accuracy. As shown in figure 1, the corresponding relationship between the projector point A and the camera point C can be depicted by the so-called pixel mapping. To make sure that each camera pixel associates with one specific projector pixel at least, the resolution of the camera should be higher than that of the projector. In practice, this requirement is easy to be satisfied.

To achieve a pixel mapping, the error-distortion phase mapping, calculating by a traditional 4-step PS algorithm, is utilized as a reference. Other N-step PS algorithms can also be applied, and we just take the 4-step PS algorithm as an example. To obtain an accurate pixel mapping, the key idea of

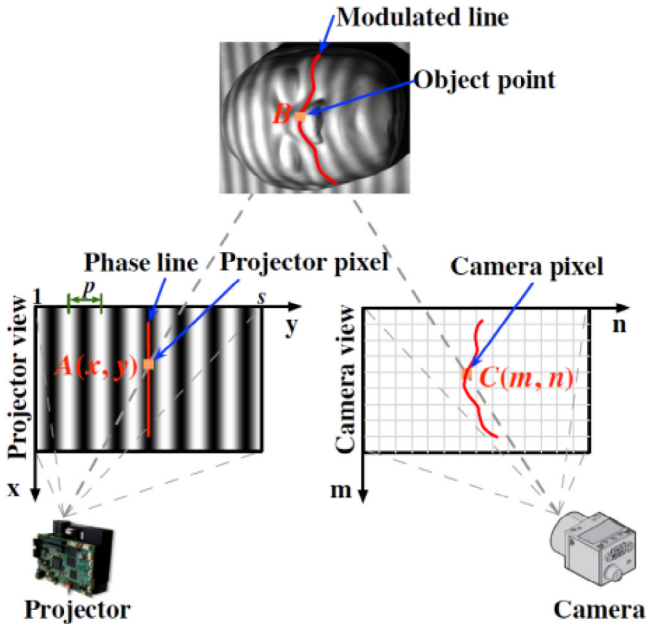

Figure 1. The schematic diagram of the light path in a PSP system. The camera pixel C can be regarded as a reflection of the object point B projected by the projector pixel A. The error-distortion value in the pixel C can be corrected by replacing with the known ground-truth value input into the projector pixel A.

extracting pixel-mapping is to utilize a minimization (optimization) taking into account the phase error distrubance.

It should be noted that the proposed pixel mapping is quite different from conventional direct pixel mapping. The proposed pixel mapping is not a direct pixel mapping but also includes error correction. The error correction is implicit in the accurate computation of pixel mapping considering the influence of phase error. However, conventional direct pixel mapping did not consider phase error and it assumed no phase error, hence it is inaccurate, which is disturbed by phase error. To compute an accurate pixel mapping, a phase error formulation is introduced to minimize the disturbance of phase error on computing the pixel mapping. Specifically, our approach is derived as follows.

2.1. Wrapped pixel mapping extraction

In the PSP method, multiple sinusoidal PS patterns with one certain frequency are projected N-times ($N = 4$) onto an object sequentially. The deformed images captured by the camera can be expressed as

$$I_n(m,n) = a(m,n) + b(m,n)\cos\left(\varphi(m,n) + \frac{2\pi n}{N}\right), \quad (1)$$

where I_n represents the nth captured images during N-step phase shifting, a and b denote the intensity bias and contrast respectively, (m, n) is the pixel coordinate of a point on the imaging plane of the camera (see figure 1), and φ is the wrapped phase can be calculated by

$$\varphi(m,n) \cong -\arctan\frac{\sum_{n=0}^{n=N-1} I_n(m,n)\sin\frac{2\pi n}{N}}{\sum_{n=0}^{n=N-1} I_n(m,n)\cos\frac{2\pi n}{N}}, N = 4. \quad (2)$$

Equation (2) gives the principle of the 4-step PS algorithm. As equation (2) involves an arctangent function, it provides the modulo 2π phase. Hence, phases calculated by equation (2) have inherent ambiguity, which are called wrapped (or relative) phases. Based on the wrapped phases, pixel positions are also wrapped. This ambiguity can be removed later by unwrapping discussed in section 2.2.

Phase error just exists in $\varphi(m,n)$. In contrast, the ideal error-free (ground-truth) phase $\varphi_t(x, y)$ embedded in the projected patterns are given by equation (3):

$$\varphi_t(x,y) = \varphi_t(y) = \frac{2\pi}{p}y, \quad (3)$$

where $\varphi_t(x, y)$ is the ideal error-free (ground-truth) phase coded by the projected pattern, p is the fringe period (see figure 1), and (x, y) is the projector pixel that illuminates the camera pixel (m, n). Note that, the phase distribution of $\varphi_t(x, y)$ is independent of the x coordinate. This is because in our derivation, the projected patterns only vary in the horizontal, as shown in the projector view in figure 1. And in reverse, with vertical patterns, the derivation is also true.

According to equation (3), the ideal error-free phase only depends on the y. Hence, for an error-distorted phase $\varphi(m,n)$, if its accurate corresponding y can be obtained, we can use the error-free $\varphi_t(y)$ to replace and correct $\varphi(m,n)$, then the phase error can be corrected. Hence, mapping a camera pixel (m,n) to a projector phase line y is going to help the correction of phase error.

To compute an accuracy y, we aim to minimize the disturbance of phase error on computing y; the detailed method is described as follows.

First, the phase error $\Delta\varphi(m,n)$ in camera pixel (m, n) can be straightforwardly formulated in equation (4) by subtracting the ideal error-free (ground-truth) phase $\varphi_t(x, y)$ from the error-distorted phase $\varphi(m,n)$. According to equations (2) and (3), we have

$$\Delta\varphi(m,n) = \left(\varphi(m,n) + 2\pi\left(\frac{y}{p} - 1\right)\right) - \varphi_t(y), \quad (4)$$

where $\left(\frac{y}{p} - 1\right)$ is the number of fringe periods that have been experienced when approaching the pixel y, and $\frac{y}{p}$ denotes obtaining the closest integer value no less than $\frac{y}{p}$. In equation (4), $\varphi(m,n)$ is the wrapped phase in 2π, while $\varphi_t(y)$ is the unwrapped phase. To make it convenient to compare the unwrapped phase $\varphi(m,n)$ and the wrapped phase $\varphi_t(y)$, we added $2\pi\left(\frac{y}{p} - 1\right)$ to $\varphi(m,n)$ to unwrap $\varphi(m,n)$. (m, n) and (x, y) is just a pair of pixel-mapping as shown in figure 1.

Second, according to the phase error analysis in [7], for the 4-step PS algorithm, the phase error $\Delta\varphi(m,n)$ can also be formulated as

$$\Delta\varphi(m,n) = -c\sin(4\varphi_t(y)), \quad (5)$$

where c denotes the amplitude of the phase error, which can be easily estimated from the phase error distribution of the reference plane, as discussed in [7]. We directly use the region within the camera range but outside the measured object to obtain c, as do the authors in [28], and as shown in the orange

line in figure 5(a). The phase error formulation in equation (5) is the hypothesis behind the proposed method, which is based on the phase error analysis in [7], and has been validated in extensive studies [18]. Based on this hypothesis, an accurate equation (equation (6)) for solving y that considers phase error disturbance can be established later.

As equations (4) and (5) both represent phase error $\Delta\varphi\,(m,n)$, combining these two equations, we can construct equation (6) with the only unknown y, by subtracting equation equations (5) from (4), as

$$E\,(y)=\left(\varphi(m,n)+2\pi\left(\frac{y}{p}-1\right)-\varphi_t(y)+\ c\sin(4\varphi_t\,(y))\right)^2=0. \tag{6}$$

So far, y is still unknown for its underlying (m, n). To seek for the y coordinate for each (m, n), we suppose that y_k is the corresponding position from which the projected pixel is projected onto (m, n), and find the value of $y_k = y$ by minimizing equation (6). As mentioned above, the y coordinate can be uncovered by minimizing $E(y_k)$ in equation (6), that is

$$y=\arg\min_{y_k}E\,(y_k)\,,1\leqslant y_k\leqslant s, \tag{7}$$

where s is the pattern's horizontal width (see figure 1).

From equations (6) and (7), it can be seen that, the effect of phase error is taken into account when solving y, by introducing the phase error formulation in equation (5). By this means, we aim to eliminate the adverse effect of phase error on computing the pixel mapping, and obtain an accurate pixel mapping in the end.

Note that as $\varphi(m, n)$ is modulated within 2π, $E(y_k)$ also repeats its minimum value in a regular interval of p. Hence, by minimizing $E(y_k)$ in equation (6), the coordinate can be uncovered in a wrapped form with a periodicity of p. Such periodicity is shown in figure 2(c).

In practice, to explicitly highlight the extreme value, by taking the reciprocal of $E(y_k)$, $P(y_k)$ is constructed and we maximize it for searching y, that is $y^*=\arg\max_{y_k}P\,(y_k)=\arg\max_{y_k}\frac{1}{E(y_k)+\epsilon}$:

$$1\leqslant y_k\leqslant s, \tag{8}$$

where ε is an extremely small number in case of division by zero. Note that as the periodicity nature of $E\,(y_k)$, we can find a series of maxima when applying equation (8), as shown in figure 2(c). As these maxima have p periodicity, the wrapped coordinate is the remainder of dividing any of these maxima by p. Hence, so far, the pixel-mapping is still called wrapped pixel-mapping. And we use y^* to differentiate it with the unwrapped coordinate y. The unwrapped coordinate y just hides in one of these maxima. To find the unwrapped y, the details is given in section 2.2.

$P(y_k)$ straightforwardly represents how likely y_k equals to the unknown projector coordinate y. Hence, we say $P(y_k)$ as the confidence function. This optimization enables the proposed method to retrieve an exact pixel mapping, from error-distorted phases.

Figure 2 shows an example of the wrapped coordinate extracting (optimization). For an experimental camera pixel (m, n) in figure 2(b), its error-distorted phase $\varphi(m, n)$ calculated by equation (2) were submitted into equation (8). With y_k going through 1 to s, the variation regularity of $P(y_k)$ is shown in figure 2(c). As shown in figure 2(c), the confidence function $P(y_k)$ have maxima when y_k is equal to 388, 407, 426, …, with the period $p = 19$ pixels. By traversing all of the camera pixels, we can obtain a wrapped pixel mapping.

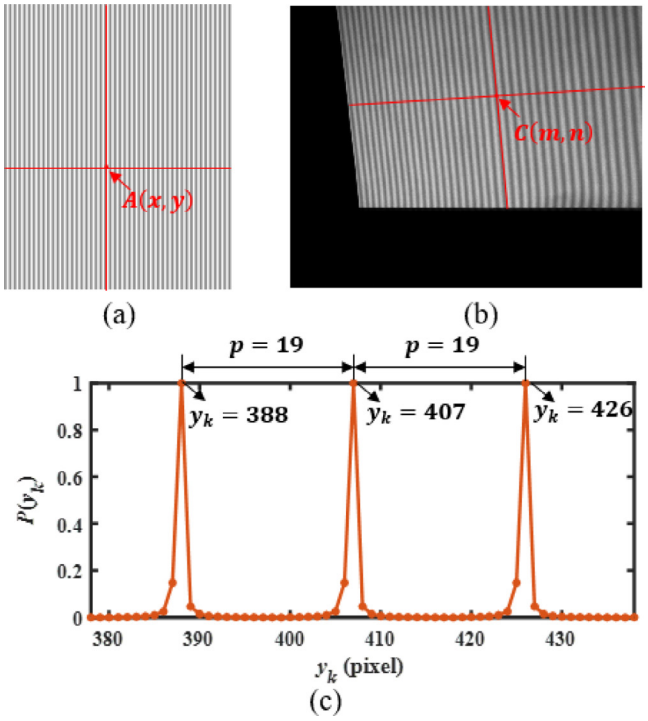

Figure 2. An example explaining the principle of the wrapped pixel mapping extraction. The fringe period p used in the example is 19 pixels. The projector pixel $A(x, y)$ in (a) is projected into $C(m, n)$ in (b). y_k traverses through the range of 1 to s to indicate the periodicity of $P(y_k)$. Note that the function values are normalized within 0 to 1 to be comparable.

2.2. Pixel mapping unwrapping

For pixel mapping unwrapping, the proposed method requires at least two sequence of traditional PS patterns, $2 \times 4 = 8$ patterns in total, for the 4-step algorithm. However, previous phase unwrapping methods usually require more patterns to project [12, 18, 24].

The key idea of the pixel mapping unwrapping is to break this periodicity of $P(y_k)$. If p_1 and p_2 are co-prime, the maximum value of the product of $P_1(y_k)$ and $P_2(y_k)$ would be repeated with the period of p_1p_2. Hence, we used two co-prime fringe periods p_1 and p_2 to emulate a longer equivalent period p_1p_2. Based on this, another confidence function is defined as

$$P^U\,(y_k)=P_1\,(y_k)\times P_2\,(y_k)\,. \tag{9}$$

The maximum point of $P^U\,(y_k)$ denotes the unwrapped pixel position y, that is

$$y=\arg\max_{y_k}P^U\,(y_k)\,,\ 1\leqslant y_k\leqslant s. \tag{10}$$

An example of the pixel mapping unwrapping is shown in figure 3. In figure 3(a), for the same camera pixel (m_0, n_0) in

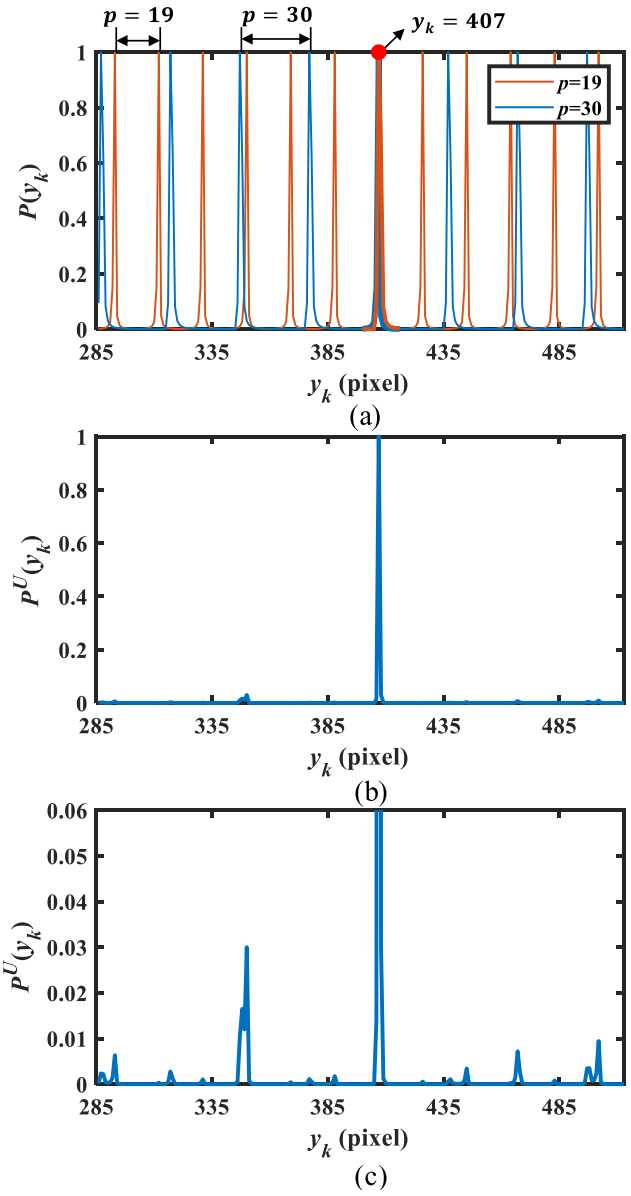

Figure 3. The process of the pixel mapping unwrapping, for the same camera pixel $C(m, n)$ as shown in figure 2(b). Two patterns with co-prime fringe periods $p_1 = 19$ pixels and $p_2 = 30$ pixels are used for unwrapping, and their related confidence functions $P_1(y_k)$ and $P_2(y_k)$ are shown in (a). The product of $P_1(y_k)$ and $P_2(y_k)$ is calculated as $P^U(y_k)$ in (b). The global maximum point $y_k = 407$ of $P^U(y_k)$ represents the unwrapped pixel position. The enlarged view of (b) where $P^U(y_k)$ scales from 0 to 0.06 is shown in (c).

figure 2(a), the local maxima of $P_1(y_k)$ and $P_2(y_k)$ coincide at $y_k = 407$, leading to a global maximum of $P^U(y_k)$ at the same point of $y_k = 407$. Therefore, the unwrapped pixel position y related to (m, n) is 407. In this example, the local maximum in $P_1(y_k)$ that coincides with $P_2(y_k)$ is just the unwrapped result. Note that in practice, the two local maxima may be inconsistent with a very small interval, due to phase error. As the phase error is very small as shown in our experiments, in this case, we find two closet maxima between $P_1(y_k)$ and $P_2(y_k)$, and the position of local maximum in $P_1(y_k)$ closest to the local maximum in $P_2(y_k)$ is just the unwrapped result.

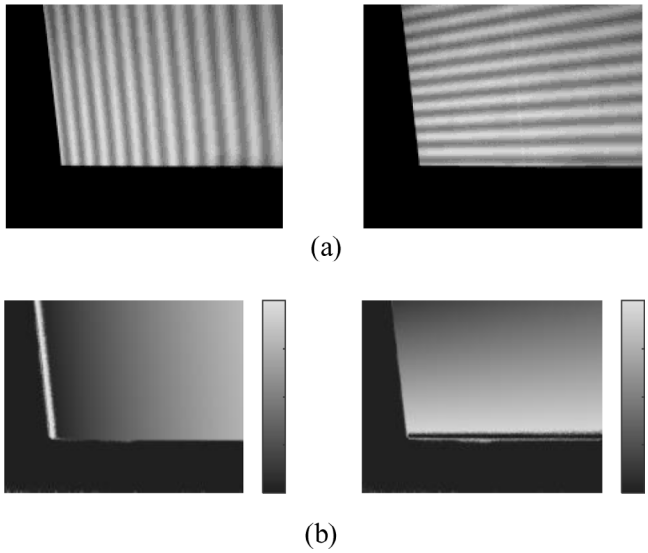

Figure 4. The result of the pixel mapping. (a) shows the captured images for mapping the column position (left) and the row position (right). (b) shows the unwrapped pixel mapping with the same gray value corresponding to the same projector column (left) and row (right). Pure white pixels mean 'uncertain'. Note that there are no uncertain pixels in the zone for measurement.

Applying the above operation for all of the camera pixels, the unwrapped pixel-mapping can be obtained.

Figures 4 and 5 show examples of the pixel mapping unwrapping with a flat board and a curve (the vase's surface), respectively. Two co-prime fringe periods $p_1 = 19$ pixels and $p_2 = 30$ pixels were used. To show the effectiveness of the pixel mapping, reconstructed images (figures 5(c) and (f)) were established by submitting the pixel mapping into equation (1). Compared with the initial images (figures 5(a) and (d)), the reconstructed images are more evenly and finely filled with sinusoidal fringes. The intensity distribution of the cross line shown in figure 5(h) also stand by this conclusion.

Note that one of the two co-prime fringe periods must be an odd number. Although the odd fringe number may affect the symmetry of sinusoidal signals, the effect on the measurement results is very small, as shown in our experiments. In addition, in some phase unwrapping methods, there is no requirement that the fringe periods should be odd, such as the multi-frequency method in [12]. However, these unwrapping methods increase the number of projections. This is very inconvenient and can reduce efficiency.

2.3. Pixel mapping-based phase error correction

The pixel mapping reveals the correspondence between the camera pixel $C(m, n)$ and its underlying projector point $A(x, y)$; see figures 1 and 6. The phase information in projector point is ideal (error-free), and is already known in equation (3). Hence, with an unwrapped pixel-mapping and according to equation (3), the error-distorted unwrapped phase extracted in each camera pixel can be directly corrected to $\Phi_c(m, n)$:

$$\Phi_c(m, n) = \varphi_t(y) = \frac{2\pi}{p} y, \tag{11}$$

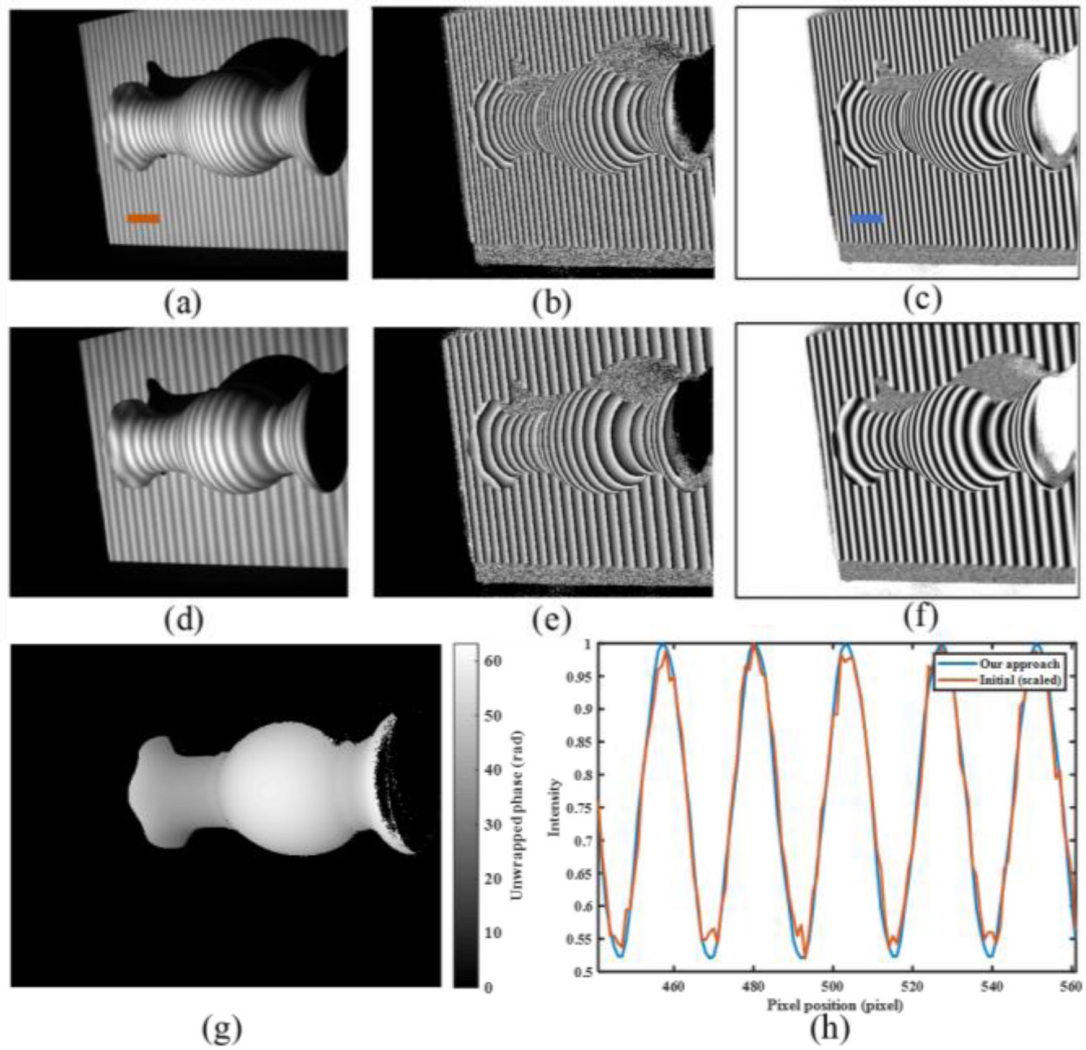

Figure 5. A vase instance reveals the specific procedures of pixel mapping unwrapping. (a) and (d) show one of the captured images with co-prime fringe periods $p_1 = 19$ pixels and $p_2 = 30$ pixels respectively. Due to the optical aberration, the difference between the two fringe periods should be larger than 5 pixels [23]. (b) and (e) show the extracted wrapped pixel mapping from (a) and (d) respectively. (c) and (f) show reconstructed images of (a) and (d) by submitting the pixel mapping into equation (1). (g) shows the unwrapped pixel mapping by using the two co-prime fringe periods. (h) shows intensity distribution of the cross line between captured image (a) and reconstructed images (c). The cross line is the orange and blue line shown in figures (a) and (c) respectively.

where $\Phi_c(m,n)$ denotes the corrected unwrapped phase in camera pixel (m, n). Note that only the y coordinate is sufficient to access the ideal phase, as the PS pattern only varies its value along one direction (see figure 1).

The difference between the proposed method and conventional compensation methods are shown in figure 6. The proposed method corrects errors by online replacement with the help of phase error formulation and with reference to the error-free ideal phase mapping, while the conventional methods compensate errors by subtracting the pre-estimated imprecise phase errors. The proposed method is online because it is implemented by using only the off-the-shelf PS patterns required for measurement, and no additional projections are required to project. The ideal phase mapping is embedded in the projected patterns, and can be directly achieved once the projected patterns are ready. The online nature takes advantage of the proposed method requiring no additional projections. In contrast, conventional methods rely on lots of additional projections to offline pre-calibrate the phase error information for further compensation. In other words, conventional methods just use the imprecise offline pre-estimated phase errors to compensate the subsequent phase errors. There is an implicit accuracy limit for conventional methods due to the static and inaccurate nature of the offline pre-estimated phase errors. Moreover, additional projections for the offline pre-estimations make conventional methods less convenience to use. Whereas, as the ideal phase mapping is ready-made, the cumbrous additional projections are not required in the proposed method.

In conclusion, we summarize the advantages that make our method outperform conventional compensation methods as follows.

(1) High accuracy: by using a pixel mapping approach, our method makes it possible to correct phase errors in an online replacement way. This online replacement way enables the proposed method to totally eliminate phase

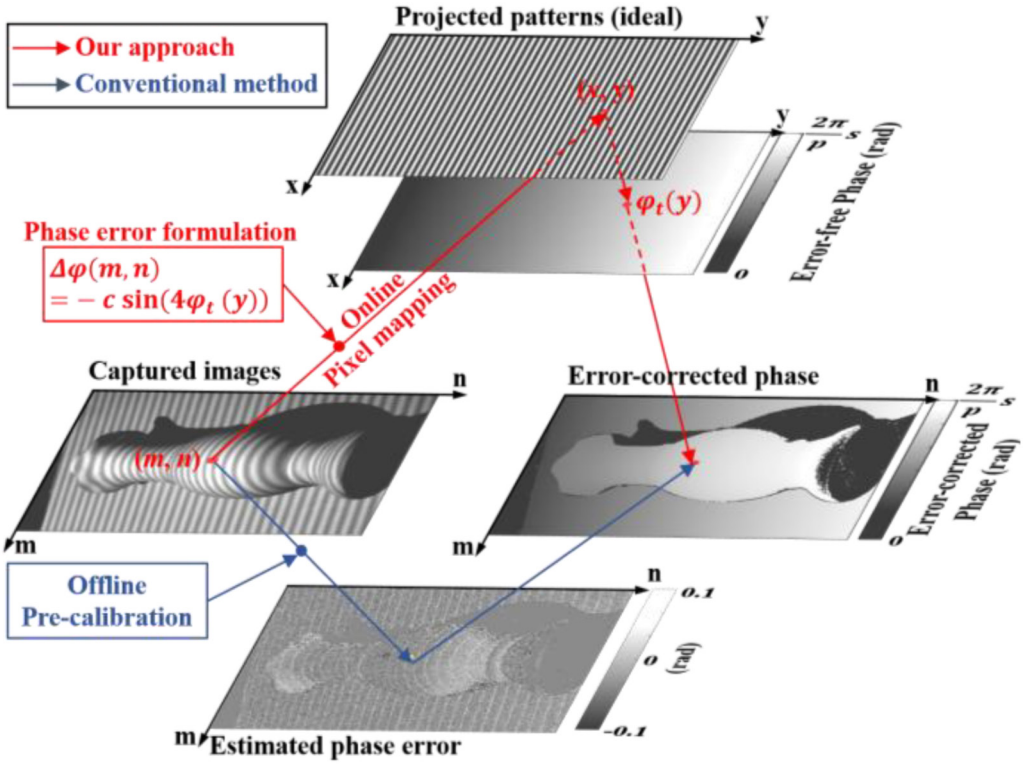

Figure 6. Difference between the key ideas of the proposed error correction method and the conventional error compensation methods. The proposed method corrects errors by online replacement with access to the error-free ideal phase mapping, while the conventional methods compensate errors by subtracting the offline pre-estimated imprecise phase errors. The pixel-mapping enables the proposed method to directly access the error-free ideal phase mapping. To obtain an accurate pixel mapping, phase error formulation is introduced to minimize the disturbance of phase error when computing the pixel mapping.

errors in theory. However, traditional compensation methods, in general, just use the imprecise offline pre-estimated phase errors to compensate the subsequent phase errors. This offline way and compensation basis limit the accuracy of conventional methods.

(2) Easy implementation: unlike traditional error compensation methods, our method does not require additional projections specially designed for error estimation and compensation. This is because the pixel-mapping establishes a shortcut from the error-distortion values to their ground-truth values. In addition, the required projection numbers for retrieving the pixel-mapping are also shrunk to a minimum, which makes sure our method is as much convenient as possible.

3. Experimental results

In this section, experimental results are presented to demonstrate the performance of the proposed method. In our experiments, to compare the performance of the proposed method with the state-of-the-art, we also employed the IP method [18], and the LUT-based method [11], which are the most typical among the existing solutions for error suppression issues. The LUT-based method is a typical method with high accuracy [29], but it requires 361 additional projections. The IP method requires only four additional projections, hence it is more convenient. In contrast, the proposed method requires no additional projections, which is the most easy implementation. As an example, all methods were implemented within the same framework of a 4-step PS algorithm. More steps could also be employed in practice. The experimental system was configured with a projector (Toshiba TDP-TW100U with a resolution of 1024 × 768 pixels) and a camera (PointGrey Flea3 FL3-U3-13E4M with a resolution of 1280 × 1024 pixels).

As mentioned in section 2, the phase error formulation in equation (5) is important in the proposed method, which is based on the conclusion in [7]. However, since the method of [7] is outdated, in our experiments we did not directly compare the proposed method with the method of [7]. In another way, as the method of [7] is a classic method, the IP method also employs the conclusion of [7]; and the LUT-based method has been compared with [7], which has been proved to have higher phase accuracy than [7]. Hence, we compared the proposed method with the newly proposed IP method and LUT-based method, which is equivalent to an indirect comparison with the method of [7].

3.1. Accuracy evaluation

We evaluated the performance of different methods in phase accuracy, as all of these methods aim to reduce the phase errors [11]. To quantitatively analyse the accuracy, we conducted an experiment with a paper attached to a flat board. First, visually, the reconstructed 3D profiles of the same paper, using

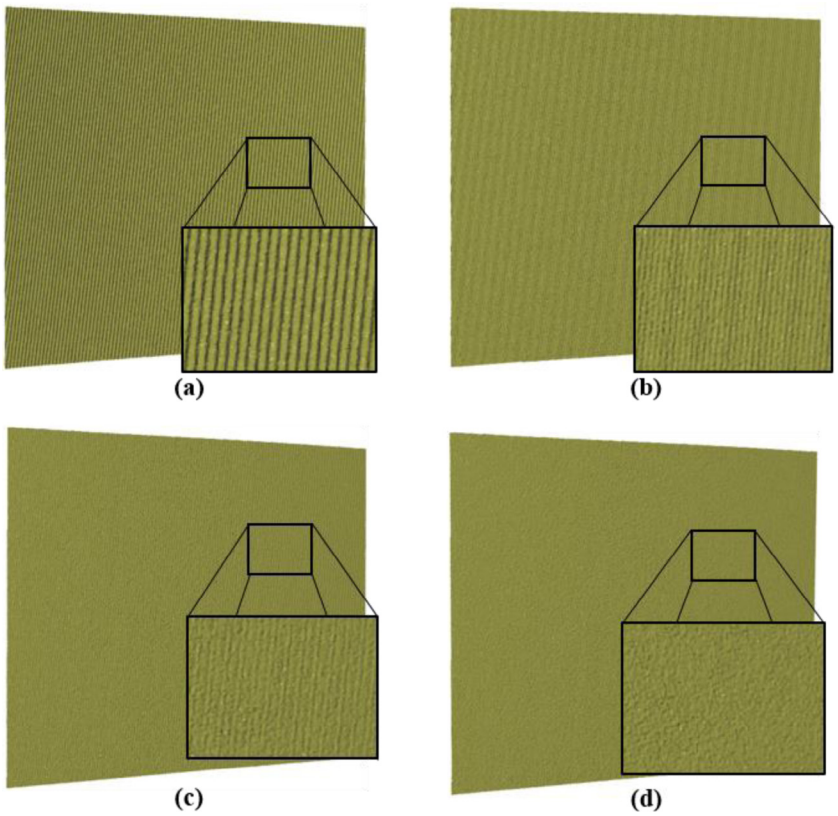

Figure 7. Comparative 3D measurement results of a paper. (a) is the result of the original four-step PS algorithm with no error compensation, (b)–(d) are the results of four-step PS algorithm with different error compensation or correction methods: the IP method, the LUT-based method, and the proposed method respectively.

different methods, are shown in figure 7. It can be observed that, compared to the conventional methods, the flatness and roughness of the paper was better preserved by the proposed method, while the wave-like errors were better reduced. The mathematical statistics in the following also stand by this conclusion.

Second, the phase accuracy was numerically evaluated by calculating the deviations from the benchmark, the retrieved phase by the 24-step PS algorithm, according to [14]. To evaluate the phase error more reliably, the experiment was repeated for three times and the average phase error was used. The residual phase errors suppression by different methods are shown in figure 8. Compared to the other methods, the maximum phase error is 3.1×10^{-3} rad with the proposed method, which is 1/5 of the LUT-based and 1/14 of the IP method.

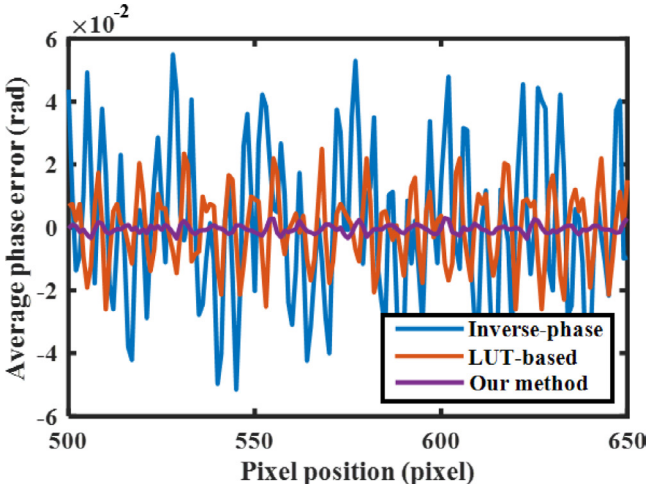

Figure 8. Phase accuracy evaluation with different methods.

3.2. Measurement results

As a practical application of the proposed approach, three plastic statues, including an ear, a portrait, and a vase were used for measurement, as shown in figure 9. These objects are typical because they have both flat and curved surfaces with edges and discontinuities. Using different methods, the reconstructed 3D profiles are shown in the 2nd to 5th columns respectively. With no treatment, distinct ripples exist in the 3D profile, which result from the nonlinear gamma. With the conventional compensation methods, these ripple-like errors can be partly alleviated, but some slight ripples are still visible. In contrast, the proposed method significantly suppressed the ripple-like errors and yielded the best performance in all measurement results. In figure 9, the period of nonlinear phenomena in the measurement results of each row looks different. This is the period of the nonlinear error, not the fringe period of the images taken by the camera. The larger the nonlinear error, the more obvious the visual effect of the nonlinear error, thus causing the period of the nonlinear error in the measurement results to look different.

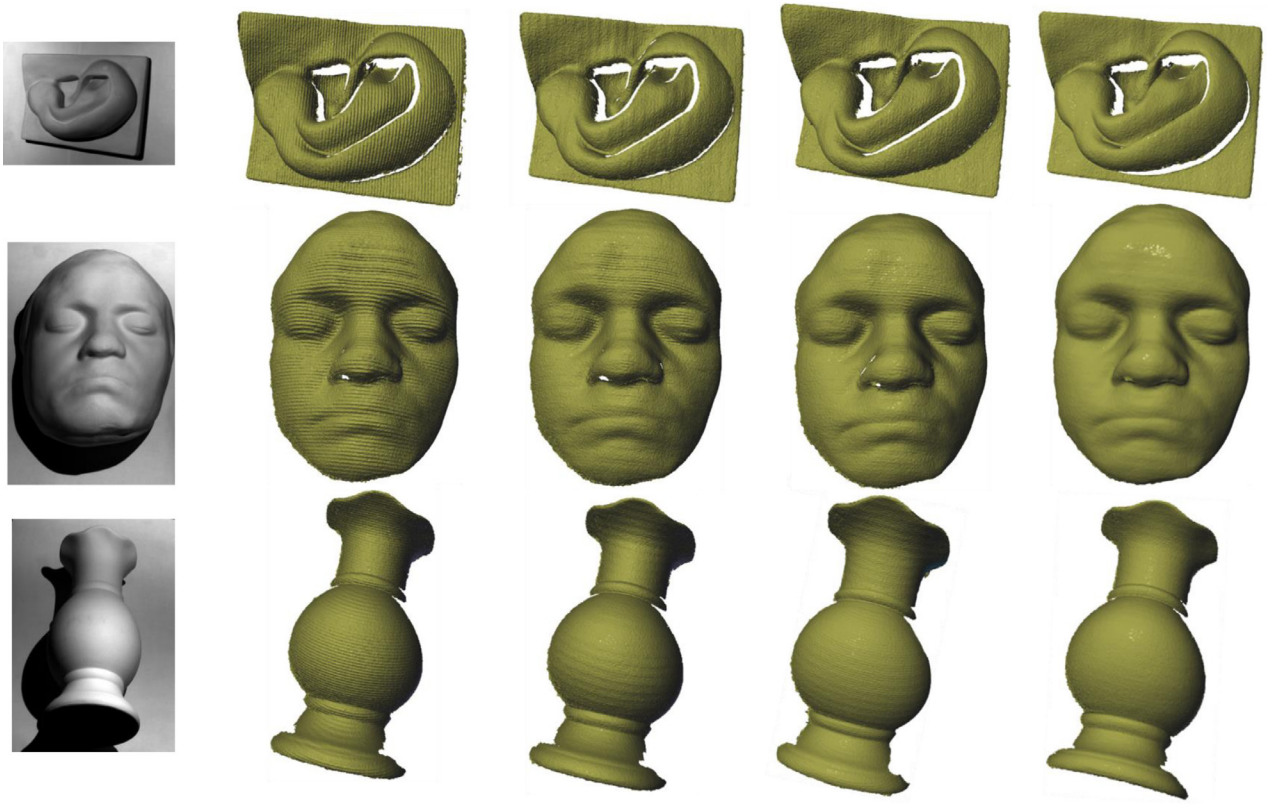

Figure 9. Experimental results of 3D surface measurement conducted in the darkroom. The first column shows the images of three measured targets. The following columns show results with no phase error compensation or correction, with the IP method, the LUT-based method and the proposed method, respectively.

It should be noted that we rotated the measurement results of the portrait and vase due to the layout of figure 9. Hence, the ripple-like errors in the measurement results of the three objects appear in different directions.

4. Conclusion

In this paper, a pixel mapping-based error correction approach was proposed to eliminate the inevitable errors in the PSP system in a convenient yet effective way. The method outperforms previous compensation methods in accuracy and it requires no additional projections. The idea of the pixel mapping makes it possible to correct phase errors in a pixel-by-pixel-replacement way, instead of in a conventional compensation way. This replacement way is the key idea of our method, which establishes a shortcut to error-free values, skipping the traditional laborious and imprecise compensation procedures. To retrieve a pixel mapping without adding projections, an optimization method using only the PS patterns was proposed. To minimize the phase error disturbance when computing the pixel mapping, a phase error formulation was introduced in the optimization method. To facilitate the acquisition of an unwrapping pixel mapping, only two sequences of patterns with co-prime periods are required. By this means, the totally required amounts of patterns are shrunk to 8, which offer improvement in flexibility, operability, and convenience. Extensive experiments conducted on three plastic statues have demonstrated the good performance of the proposed method. Conventional compensation methods were also used for comparison.

Acknowledgments

This research was supported by the National Natural Science Foundation of China (Grant Nos. 51775497, 51775498), Zhejiang Provincial Natural Science Foundation of China (Grant No. LY17F030011).

ORCID iDs

Zaixing He https://orcid.org/0000-0003-0577-8009
Peilong Li https://orcid.org/0000-0002-1622-0214
Xinyue Zhao https://orcid.org/0000-0002-7184-0985
Shuyou Zhang https://orcid.org/0000-0001-9023-5361

References

[1] Yu L, Zhang W, Li W, Pan C and Xia H 2016 Simplification of high order polynomial calibration model for fringe projection profilometry *Meas. Sci. Technol.* **27** 105202
[2] Tayebi B, Sharif F, Karimi A and Han J 2018 Stable extended imaging area sensing without mechanical movement based on spatial frequency multiplexing *IEEE Trans. Ind. Electron.* **65** 8195–203

[3] Kudo R, Usuki S, Takahashi S and Takamasu K 2012 Influence of standing wave phase error on super-resolution optical inspection for periodic microstructures *Meas. Sci. Technol.* **23** 054007
[4] Zhang S and Yau S T 2006 High-resolution, real-time 3D absolute coordinate measurement based on a phase-shifting method *Opt. Express* **14** 2644–9
[5] Srinivasan V, Liu H C and Halioua M 1985 Automated phase-measuring profilometry: a phase mapping approach *Appl. Opt.* **24** 185–8
[6] Wang Z, Nguyen D A and Barnes J C 2010 Some practical considerations in fringe projection profilometry *Opt. Lasers Eng.* **48** 218–25
[7] Pan B, Kemao Q, Huang L and Asundi A 2009 Phase error analysis and compensation for nonsinusoidal waveforms in phase-shifting digital fringe projection profilometry *Opt. Lett.* **34** 416–8
[8] Zhang S and Huang P S 2007 Phase error compensation for a 3D shape measurement system based on the phase-shifting method *Opt. Eng.* **46** 106401
[9] Zhang S 2015 Comparative study on passive and active projector nonlinear gamma calibration *Appl. Opt.* **54** 3834–41
[10] Zhang S and Yau S T 2007 Generic nonsinusoidal phase error correction for three-dimensional shape measurement using a digital video projector *Appl. Opt.* **46** 36–43
[11] Zhang C, Zhao H, Zhang L and Wang X 2015 Full-field phase error detection and compensation method for digital phase-shifting fringe projection profilometry *Meas. Sci. Technol.* **26** 035401
[12] Zuo C, Huang L, Zhang M, Chen Q and Asundi A 2016 Temporal phase unwrapping algorithms for fringe projection profilometry: a comparative review *Opt. Lasers Eng.* **85** 84–103
[13] Cai Z, Liu X, Peng X, Zhang Z, Jiang H, Yin Y and Huang S 2016 Phase error compensation methods for high-accuracy profile measurement *Meas. Sci. Technol.* **27** 045201
[14] Hoang T, Pan B, Nguyen D and Wang Z 2010 Generic gamma correction for accuracy enhancement in fringe-projection profilometry *Opt. Lett.* **35** 1992–4
[15] Hu Y, Xi J, Chicharo J F, Cheng W and Yang Z 2009 Inverse function analysis method for fringe pattern profilometry *IEEE Trans. Instrum. Meas.* **58** 3305–14
[16] Li Z and Li Y 2011 Gamma-distorted fringe image modeling and accurate gamma correction for fast phase measuring profilometry *Opt. Lett.* **36** 154–6
[17] Zhang W, Yu L, Li W, Xia H, Deng H and Zhang J 2017 Black-box phase error compensation for digital phase-shifting profilometry *IEEE Trans. Instrum. Meas.* **66** 2755–61
[18] Lei Z, Wang C and Zhou C 2015 Multi-frequency inverse-phase fringe projection profilometry for nonlinear phase error compensation *Opt. Lasers Eng.* **66** 249–57
[19] Guehring J 2001 Dense 3D surface acquisition by structured light using off-the-shelf components *Videometrics Opt. Meth. 3D Shape Meas.* **4309** 220–31
[20] Sansoni G, Carocci M and Rodella R 1999 Three-dimensional vision based on a combination of gray-code and phase-shift light projection: analysis and compensation of the systematic errors *Appl. Opt.* **38** 6565–73
[21] Song Z, Chung R and Zhang X 2013 An accurate and robust strip-edge based structured light means for shiny surface micro-measurement in 3D *IEEE Trans. Ind. Electron.* **60** 1023–32
[22] Moreno D and Taubin G 2012 Simple, accurate, and robust projector-camera calibration *Proc. 2nd Int. Conf. 3D Imaging Modeling Processing, Visualization, Transmission* pp 464–71
[23] Gupta M and Nayar S K 2012 Micro phase shifting *Proc. IEEE Conf. Comput. Vis. Pattern Recognit.* pp 813–20
[24] Wang Z 2015 An imaging and measurement system for robust reconstruction of weld pool during arc welding *IEEE Trans. Ind. Electron.* **62** 5109–18
[25] You J and Joo K N 2012 Minimization of spectral phase errors in spectrally resolved white light interferometry by the iterative least-squared phase-shifting method *Meas. Sci. Technol.* **23** 125203
[26] Wei Y, Wu C, Wang Y and Dong Z 2015 Efficient shape reconstruction of microlens using optical microscopy *IEEE Trans. Ind. Electron.* **62** 7655–64
[27] Mao C, Lu R and Liu Z 2018 A multi-frequency inverse-phase error compensation method for projector nonlinear in 3D shape measurement *Opt. Commun.* **419** 75–82
[28] Xing S and Guo H 2018 Correction of projector nonlinearity in multi-frequency phase-shifting fringe projection profilometry *Opt. Express* **26** 16277–91
[29] Babaei A, Saadatseresht M and Kofman J 2017 Exponential fringe pattern projection approach to gamma-independent phase computation without calibration for gamma nonlinearity in 3D optical metrology *Opt. Express* **25** 24927–38